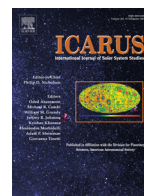




Contents lists available at ScienceDirect

Icarus

journal homepage: www.elsevier.com/locate/icarus

Three-dimensional radar imaging of structures and craters in the Martian polar caps

Nathaniel E. Putzig^{a,*}, Isaac B. Smith^a, Matthew R. Perry^a, Frederick J. Foss II^b,
Bruce A. Campbell^c, Roger J. Phillips^d, Roberto Seu^e

^a Planetary Science Institute, 1546 Cole Boulevard, Suite 120, Lakewood, CO 80401, USA

^b Freestyle Analytical and Quantitative Services, LLC, 2210 Parkview Drive, Longmont, CO 80504, USA

^c Center for Earth and Planetary Studies, National Air and Space Museum, Smithsonian Institution, MRC 315, 4th and Independence Ave, SW, Washington, DC 20560, USA

^d Department of Earth and Planetary Sciences and McDonnell Center for the Space Sciences, Washington University in St. Louis, St. Louis, MO 63130, USA

^e DIET Department, Sapienza University of Rome, Via Eudossiana, 18, 00184 Rome, Italy

ARTICLE INFO

Article history:

Received 1 April 2017

Revised 21 July 2017

Accepted 18 September 2017

Available online xxx

Keywords:

Mars
Mars, polar caps
Mars, climate
Mars, interior
Ices
Cratering
Radar observations

ABSTRACT

Over the last decade, observations acquired by the Shallow Radar (SHARAD) sounder on individual passes of the Mars Reconnaissance Orbiter have revealed the internal structure of the Martian polar caps and provided new insights into the formation of the icy layers within and their relationship to climate. However, a complete picture of the cap interiors has been hampered by interfering reflections from off-nadir surface features and signal losses associated with sloping structures and scattering. Foss et al. (The Leading Edge 36, 43–57, 2017, <https://doi.org/10.1190/tle36010043.1>) addressed these limitations by assembling three-dimensional data volumes of SHARAD observations from thousands of orbital passes over each polar region and applying geometric corrections simultaneously. The radar volumes provide unprecedented views of subsurface features, readily imaging structures previously inferred from time-intensive manual analysis of single-orbit data (e.g., trough-bounding surfaces, a buried chasma, and a basal unit in the north, massive carbon-dioxide ice deposits and discontinuous layered sequences in the south). Our new mapping of the carbon-dioxide deposits yields a volume of 16,500 km³, 11% larger than the prior estimate. In addition, the radar volumes newly reveal other structures, including what appear to be buried impact craters with no surface expression. Our first assessment of 21 apparent craters at the base of the north polar layered deposits suggests a Hesperian age for the substrate, consistent with that of the surrounding plains as determined from statistics of surface cratering rates. Planned mapping of similar features throughout both polar volumes may provide new constraints on the age of the icy layered deposits. The radar volumes also provide new topographic data between the highest latitudes observed by the Mars Orbiter Laser Altimeter and those observed by SHARAD. In general, mapping of features in these radar volumes is placing new constraints on the nature and evolution of the polar deposits and associated climate changes.

© 2017 Elsevier Inc. All rights reserved.

1. Introduction

The icy layers of Planum Boreum and Planum Australe, the north and south polar caps of Mars, have been studied from orbit for decades, but the record of climate change that they encode is still not fully understood (Byrne, 2009). Two orbiting radar sounders, the Mars Advanced Radar for Subsurface and Ionosphere Sounding (MARSIS) onboard Mars Express and the Shallow Radar

(SHARAD) onboard Mars Reconnaissance Orbiter (MRO), have been probing the cap interiors since 2005 and 2006, respectively. MARSIS results have established the gross internal geometries of both polar caps (Plaut et al., 2007; Selvans et al., 2010) whereas SHARAD results have revealed finer-scale layering and structures (Seu et al., 2007a; Phillips et al., 2008).

In Planum Boreum, SHARAD mapping with more extensive coverage (Putzig et al., 2009) showed that the broadly continuous strata, delineated by packets of finely spaced reflecting layers separated by relatively homogeneous inter-packet zones, is pervasive. Comparisons to results from climate models (Laskar et al., 2002; Levrard et al., 2007) suggested that each sequence may correspond to a ~1-Ma orbital cycle (Phillips et al., 2008; Putzig et al., 2009).

* Corresponding author.

E-mail addresses: nathaniel@putzig.com (N.E. Putzig), ibsmith@psi.edu (I.B. Smith), mperry@psi.edu (M.R. Perry), foss@airmail.net (F.J. Foss II), campbellb@si.edu (B.A. Campbell), phillips@levee.wustl.edu (R.J. Phillips), roberto.seu@uniroma1.it (R. Seu).

<https://doi.org/10.1016/j.icarus.2017.09.023>

0019-1035/© 2017 Elsevier Inc. All rights reserved.

A low degree of basal deflection (<100 m) indicated either a transient state of compensation in the mantle (unlikely) or a much thicker (>~300-km) elastic lithosphere than had previously been considered (Phillips et al., 2008). Mapping of structures below spiral troughs showed them to be dune-like, poleward-migrating features that result from a long-lived interaction of winds with icy surface materials (Smith and Holt, 2010; Smith et al., 2013). In addition, Holt et al. (2010) delineated unconformities and mapped a buried chasma to the east of the topographic saddle that connects Gemina Lingula to the main lobe of the north polar layered deposits (NPLD), while showing that Chasma Boreale is a long-lived feature and not the result of erosion into pre-existing layers. Beneath the NPLD, SHARAD data show transitions from nearly radar-transparent ice to a basal unit yielding diffuse reflections under most of the main lobe (Brothers et al., 2015; Nerozzi and Holt, 2017) and to a presumably rocky substrate yielding strong reflections elsewhere. Deeper, strong reflections obtained by MARSIS show that the basal unit extends down to the same rocky substrate (Selvans et al., 2010), but SHARAD generally obtains no reflections there, its higher frequencies apparently attenuated within the basal unit. This radar basal unit corresponds to the sand-rich rupes and cavi geologic units of Tanaka and Fortezzo (2012) at the base of the NPLD that were identified previously with surface imagery (Byrne and Murray, 2002; Fishbaugh and Head, 2005).

In Planum Australe, SHARAD data show regionally discontinuous radar layering, with truncation at or near the surface in some areas (suggesting previous widespread erosion and a lack of substantial deposition in the current era) (Seu et al., 2007a) and enigmatic low-reflectivity zones in other areas (Phillips et al., 2011). The low-reflectivity zones atop Australe Mensa nearest the pole were determined to be composed of CO₂ ice (Phillips et al., 2011) that appears to have accumulated during three separate episodes of atmospheric collapse (Bierson et al., 2016). These deposits contain more than enough CO₂ to double the current atmospheric pressure if sublimated. Elsewhere in the south polar layered deposits (SPLD), regional mapping efforts combined with surface imagery have gleaned some insight into the deeper interior (e.g., Milkovich et al., 2009) and suggest that the layers are more pervasive than seen in the radar data. However, some combination of signal scattering and attenuation has made it challenging to map layers more broadly across the southern cap with the available radar observations (Campbell et al., 2015).

While detailed mapping of internal structures in the northern cap has been more successful than in the south, doing so in either hemisphere with collections of data from individual radar passes is laborious and hindered by scattering and the interference of off-nadir surface reflections from spiral troughs and other variable topography. Reflected radar signals that return to the spacecraft (“returns” hereinafter) are dominated by those coming from the nadir track (the vertical projection of the spacecraft position to the surface), which usually arrive first. Returns from off-nadir surface structures, termed “clutter,” usually arrive later and may be mistaken for or interfere with nadir returns from subsurface interfaces. In areas where surface or subsurface interfaces are sloped, a common geometry near the spiral troughs of both polar caps, the first returns may be from off-nadir locations with no returns from nadir, yielding distorted profiles that are difficult to interpret. Focused processing enabled by along-track Doppler frequency shifts is typically applied to single-pass observations (i.e., two-dimensional profiles; see next section). Such processing greatly enhances along-track resolution by constructing a synthetic aperture (antenna) in that direction and can be effective in suppressing clutter and in improving positioning along track, but the cross-track components cannot be similarly focused to improve resolution.

One means to address these problems is to gather data from many closely spaced orbital passes into a single volume and apply

a three-dimensional (3-D) image-correction process that has been best developed in the field of seismic data processing (Yilmaz, 1987; Gray et al., 2001). This treatment enhances the signal-to-noise ratio (SNR) by combining returns from overlapping and nearby tracks while placing scattered along-track and cross-track returns into their proper source locations, thereby revealing the true geometry of surface and interior structures. In the following sections, we discuss SHARAD observations and provide an overview of the methods used by Foss et al. (2017) to produce SHARAD 3-D volumes encompassing the north and south polar caps. We then show results from the two polar data volumes and describe our initial scientific findings stemming from the use of these unique datasets.

2. SHARAD observations

SHARAD is a chirped-pulse sounding radar with a 10-MHz bandwidth centered at 20 MHz. Range (~vertical) resolution (i.e., the radar wavelength) is 15 m in free space and finer in the subsurface, depending on the material properties (Seu et al., 2007b). For nearly pure water ice with a real permittivity, ϵ' , of 3.15 as is inferred for the NPLD (Picardi et al., 2005; Phillips et al., 2008; Grima et al., 2009), the range resolution is reduced to $15/\sqrt{\epsilon'} = \sim 8$ m. A greater proportion of lithic inclusions, likely the case for Planum Boreum basal units and in portions of Planum Australe, will increase the real permittivity and thereby yield a finer range resolution. Increased pore space or a different composition (e.g., CO₂ ice, such as in the low-reflectivity zones near the south pole) may result in a decrease of real permittivity and a coarser range resolution. With the MRO orbit at a 250–320 km altitude, the lateral resolution at the surface is ~3–6 km, reducible in the along-track direction to 0.3–1.0 km in focused processing (Seu et al., 2007b).

Each SHARAD record contains reflections from all terrain within a large area illuminated by the antenna beam, so additional processing is used to narrow the contributing region. Along-track resolution is greatly improved by focused Doppler processing of a suite of pulses recorded as the spacecraft moves along track. Returns from several seconds of observation are used to form a synthetic aperture in which the reflections from the desired region are isolated in time delay and Doppler frequency shift, then summed to obtain the maximum SNR. Side-by-side stacking of progressive focused return traces spaced at 300–500 m along track creates a radargram (i.e., a 2-D profile image of returned radar power with distance along track on the horizontal axis and range delay time—sometimes converted to depth—along the vertical axis; see Fig. 1). For more details of 2-D radar processing methods, see the documentation for the U.S. SHARAD derived data products and references therein (Campbell and Phillips, 2014).

Bright returns in a radargram indicate strong contrasts in the dielectric properties of materials at geologic interfaces while providing geometric information that reveals subsurface structure. Mineralogical differences may strongly attenuate radar waves, and changes in return strength along a dipping horizon can be used to characterize the loss properties (e.g., Campbell et al., 2008; Watters et al., 2007). In the polar terrains of Mars, reflections likely arise from dielectric contrasts between ice layers with different compositions (H₂O or CO₂) or degrees of dust or lithic loading (e.g., Nunes and Phillips, 2006; Grima et al., 2009; Putzig et al., 2009).

3. Methods

Here we provide an overview of the procedures used by Foss et al. (2017) to take the SHARAD observations from collections of 2-D profiles to geometrically corrected 3-D volumes for each polar region. More details are available in the cited references.

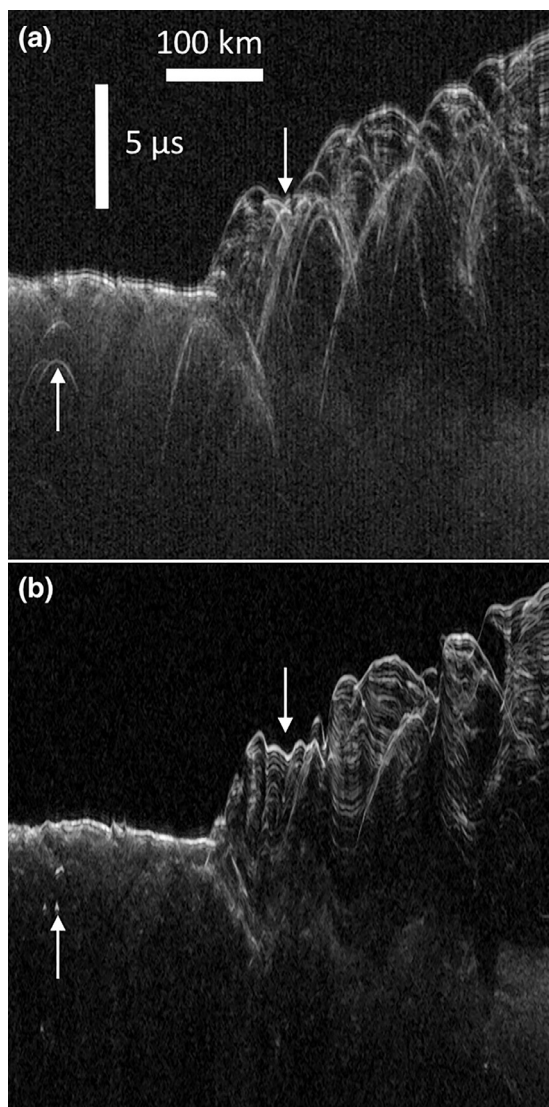


Fig. 1. Radargrams (profiles of power in delay time vs. along-track distance) for SHARAD observation 19777-01 in a trough-rich area of the NPLD. (a) Echoes in the unfocused image appear as hyperbolic arcs centered on ground features. (b) 2-D focusing combines echoes with appropriate phase and time-delay shifts to produce a view of surface and subsurface reflectors in finer along-track resolution and higher SNR. Arrows show effects of focusing for an off-nadir surface clutter source (left) and for a surface depression (right).

Crucial to focused processing of orbital radar data is an accurate representation of the spacecraft velocity and the local surface slope. Horizontal reflectors directly below the spacecraft typically yield the strongest surface and subsurface returns. As an interface dips away from horizontal, the focusing becomes less effective, and at high slope angles interfaces may disappear entirely due to the geometric limitation imposed by SHARAD's 135- μ s range window. Clutter signals from features off the nadir track of the spacecraft (e.g., crater walls, polar troughs) are often difficult to uniquely identify in a single radargram since they may focus well in 2-D (Fig. 1). A useful discriminator between clutter and subsurface returns is their relative “move-out.” Typically, off-nadir surface features will shift much more in time delay between nearby, parallel ground tracks than near-horizontal reflectors at nadir. This type of analysis was demonstrated with data from the Apollo Lunar Sounder Experiment (Maxwell and Phillips, 1978; Peeples et al., 1978) using a graphical approach. For SHARAD, Mars elevation data and a model of the radar have been used to produce synthetic radargrams for identifying clutter (Choudhary et al., 2016).

Over the course of the MRO mission, the coverage density of SHARAD observations in the polar regions has increased to the point where it has become feasible to treat each polar dataset as a 3-D volume rather than as a collection of 2-D profiles. This approach provides several advantages. At orbit crossings, data from multiple observations may be summed to improve the SNR proportionally to the square root of the number of overlapping data values (demonstrated with 2-D profiles by Campbell et al., 2015). The 3-D imaging relies on a technique referred to as “migration” in seismic data processing (which usage differs in substantive ways from that employed in the field of radar processing) and described in detail below. Where features are well sampled by the radar, 3-D migration processing can unravel interfering nadir and off-nadir returns, effectively treating the latter as useful information on the geometry of off-nadir topography with respect to the nadir ground track.

Terrestrial active-source seismic surveys are designed to sample the subsurface in either a cross-sectional area (2-D acquisition with sources and receivers deployed in a line) or a volume (3-D acquisition with sources and receivers deployed in a grid). A fraction of the energy emitted by the sources that passes into the subsurface is reflected upward and recorded at receivers. The clarity of the recorded image depends on the acquisition parameters and the seismic complexity of the subsurface. In seismically complex areas, it is often necessary to apply certain processes to the data to correct geometric effects. To this end, migration has become a routine part of seismic data processing. Migration is a mathematical inversion process whereby the seismic image recorded at or near the surface is re-imaged to appear as if it were recorded directly above the subsurface points sampled by the wave field (French, 1974; Claerbout, 1985; Yilmaz, 1987; Yilmaz et al., 1987a, 1987b). Migration converts the input seismic image to one in which subsurface features appear in their proper position laterally and vertically. In addition, migration improves resolution of the image by collapsing backscattered wave-field energy to the scattering point. Many migration algorithms have been developed and implemented to account for subsurface seismic complexity of various degrees (Stolt, 1978; Gazdag, 1978; Gray et al., 2001; Bednar, 2005).

Migration algorithms often require zero-offset data, wherein sources and receivers are nominally co-located. True zero-offset seismic surveys are not typical in practice because seismic sources (e.g., dynamite, airguns) are destructive, so additional processing steps are taken to produce pseudo-zero-offset data. For SHARAD, the same antenna transmits and receives the signals, with the spacecraft typically moving less than 10 m and Doppler processing accounting for the relative motion between the spacecraft and the surface, so the polar grids of 2-D radargrams are already effective zero-offset 3-D volumes. Thus, it was possible to use zero-offset seismic processing methods to treat the SHARAD data over each polar region as a single 3-D reflectivity volume (Foss et al., 2017). As implemented, 3-D migration addresses many of the limitations of interpreting single 2-D radargrams in areas of complex topography. For example, clutter returns in 2-D are “moved” in the 3-D volume to better align these returns with the surface topography from which they were reflected. In addition, the 3-D processing further improves the SNR largely through incoherent stacking of reflectors seen in multiple tracks.

Prior to carrying out the 3-D processing, it is necessary to correct ionospheric distortions and delays of the radar returns that vary in time and space. The dense grid of SHARAD coverage proved very useful in assessing and removing the relative ionospheric delays between tracks and along each track, a critical correction aimed at preserving the range resolution of the input data. As implemented for the standard processing of SHARAD data (Campbell and Phillips, 2014), these corrections are carried out in

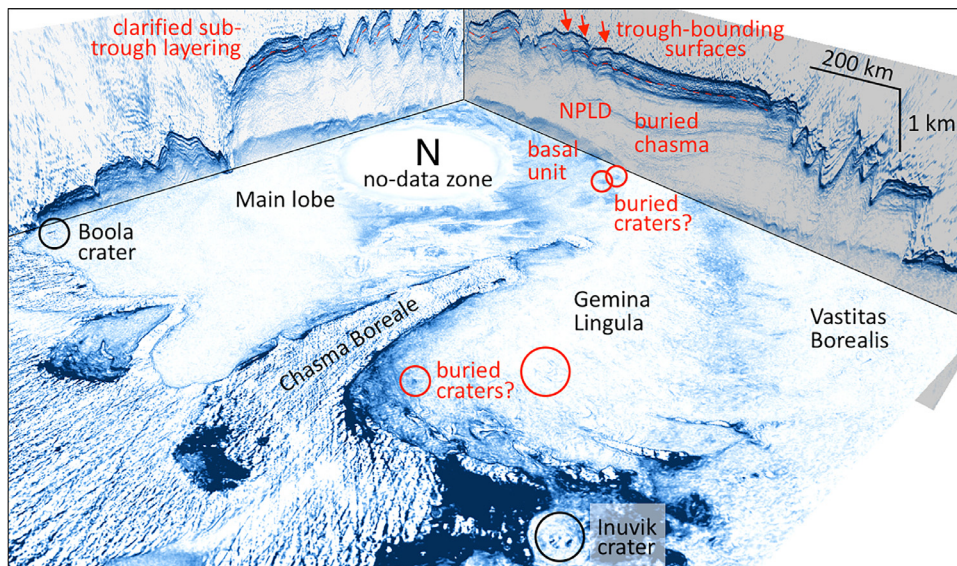


Fig. 2. Cut-away perspective view (toward 150 °E) into the depth-converted Planum Boreum SHARAD 3-D volume, showing radar-return power (blue high, white low) from previously known (black) and buried (red) features within the north polar cap. The SHARAD no-data zone is due to MRO's orbit inclination. Depth conversion assumes pure water ice ($\epsilon' = 3.15$). Scale is approximate (varies in this perspective), with vertical exaggeration of 136:1. (For interpretation of the references to color in this figure legend, the reader is referred to the web version of this article.)

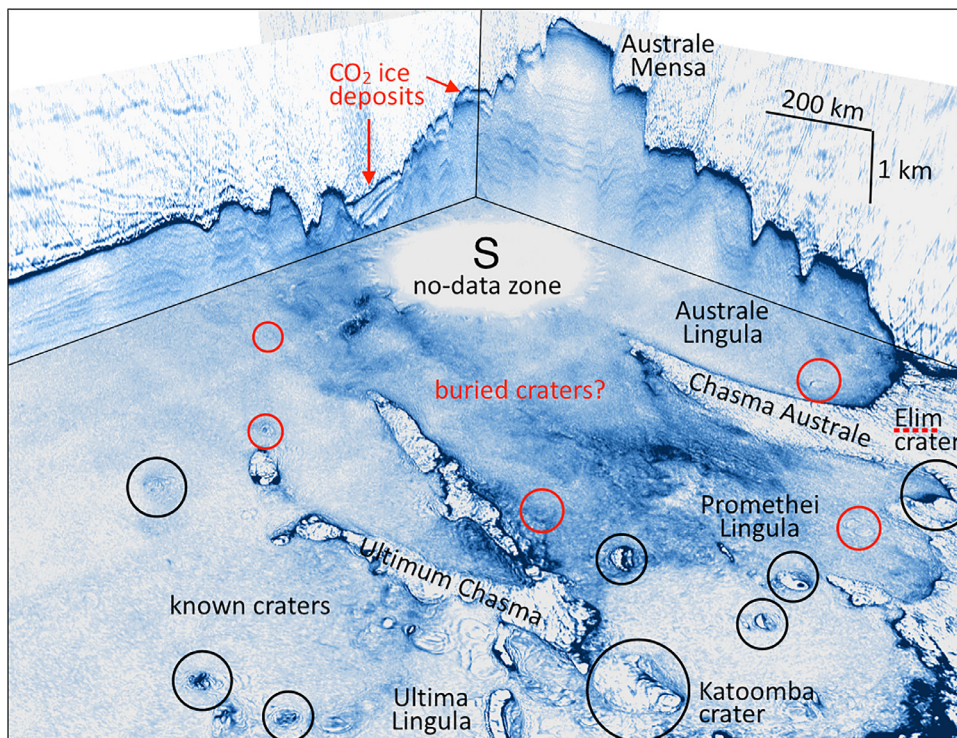


Fig. 3. Cut-away perspective view (toward 315 °E) into the depth-converted Planum Australe SHARAD 3-D volume, showing radar-return power (blue high, white low) from previously known (black) and buried (red) features within the south polar cap. The SHARAD no-data zone is due to MRO's orbit inclination. Depth conversion assumes pure water ice ($\epsilon' = 3.15$). Scale is approximate (varies in this perspective), with vertical exaggeration of 136:1. (For interpretation of the references to color in this figure legend, the reader is referred to the web version of this article.)

an autofocusing process (Campbell et al., 2014). In preparation for the 3-D imaging, we apply a so-called “demigration” process to each 2-D radargram that redistributes each sample along a hyperbolic 2-D diffraction curve (Foss et al., 2017). This step has the effect of repositioning reflectors to their zero-offset positions, resulting in a product that is similar to an unfocused radargram (e.g., Fig 1a). Next, all 2-D radargrams (2300 in the north and 2100 in the south for the current volumes) are assembled into a 3-D binning grid, wherein the grid size (475 m) is chosen close to the in-

put 2-D frame interval. While spatial aliasing is theoretically possible at these bin sizes (e.g., see p. 191–196 of Liner, 2016), the data are effectively anti-aliased along-track in the 2-D pre-processing. Subsequent to the 3-D binning, a spatial interpolation is applied to fill coverage gaps—largest on the polar-cap periphery where tracks diverge—prior to further processing that culminates in the 3-D migration step (Foss et al., 2017), which “moves” reflectors from the locations where they were recorded to their true subsurface positions.

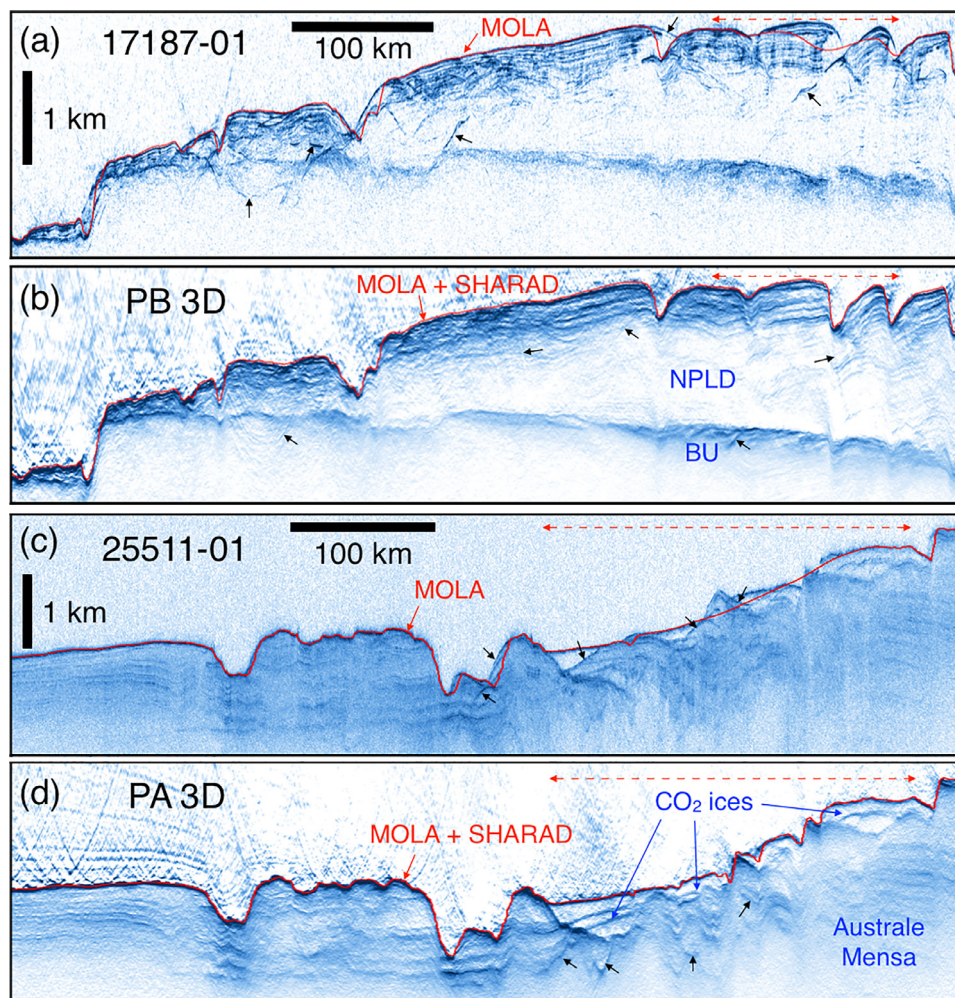


Fig. 4. (a, c) SHARAD depth profiles for single-orbit crossings compared to (b, d) profiles extracted from the corresponding 3-D volumes along the same ground tracks in Planum Boreum (a, b) and Planum Australe (c, d). 3-D imaging corrects surface and subsurface structures, separating the interfering nadir and off-nadir returns evident in the 2-D profiles, and enhancing SNR at depth but with some loss of vertical resolution. Black arrows in (a, c) indicate examples of clutter signals largely corrected by 3-D processing. Black arrows in (b, d) indicate examples of likely artifacts in the 3-D volumes due to incomplete correction of off-nadir echoes from features with inadequate SHARAD coverage. Red lines are the MOLA-derived surface profile along each ground track, replaced by the SHARAD-derived surface in (b) and (d) in the zones indicated by red dashed arrows where SHARAD observes higher latitudes than MOLA did. Depth conversion assumes pure water ice ($\epsilon' = 3.15$). See Fig. 9 for ground-track locations. (For interpretation of the references to color in this figure legend, the reader is referred to the web version of this article.)

4. Results and discussion

The geometric corrections and improved SNR afforded by these first SHARAD 3-D volumes are providing an improved understanding of the interior structure and stratigraphy of Planum Boreum and Planum Australe. Major subsurface structures that required substantial effort to map with collections of 2-D profiles (e.g., the surface of a basal unit (Brothers et al., 2015), a buried chasma (Holt et al., 2008), and a widespread shallow sequence providing evidence of a recent glaciation (Smith et al., 2016) in the north; interior layering and CO_2 ice deposits in the south (Phillips et al., 2011; Bierson et al., 2016)) are plainly visible in the volumes (Figs. 2 and 3; see also animations available at <http://sharad.psi.edu/3D>). At the same time, other features are newly imaged. In Planum Boreum, previously obscured unconformities and layered sequences below trough-rich regions above and within the basal unit (dashed red line in Fig. 2; Fig. 4a and b) provide new clues about the depositional history of the polar cap (Smith et al., 2016). In Planum Australe, many of the layers that are disrupted on individual observations can now be followed much further throughout the 3-D data volume, and geometric corrections provided by the 3-D imaging improve the view of buried structures (e.g., Fig. 4c

and d). In particular, the improved imaging of CO_2 ice deposits associated with the low reflectivity zones in Australe Mensa have allowed us to more confidently map their extents (Fig. 5). With extrapolation to geologic boundaries mapped inside the radar no-data zone surrounding the south pole, we find that these deposits contain about $16,500 \text{ km}^3$ of CO_2 ice, which is 11% larger than the previous estimate (Bierson et al., 2016) and corresponds to a mass 6% greater than that of the current Martian atmosphere. Because SHARAD does not have complete coverage over the polar regions, some artifacts occur within the radar volumes. Specifically, surface and subsurface returns are not fully corrected in areas where the reflecting features do not have sufficient coverage for complete 3-D images, such as lower ($\sim 30\%$) coverage areas near the periphery of Planum Boreum and Planum Australe and locations along the high-latitude no-data zones. Examples of such artifacts are given in Fig. 4b and d.

In addition to providing geometric corrections, the 3-D volumes allow examination of the radar data in orientations not offered by the collection of 2-D profiles, such as constant delay-time or depth slices and profiles that need not follow the orbit trajectories (e.g., Figs. 2, 3, and 7). The slice views are especially useful for examining the distinctive radar signatures associated with known,

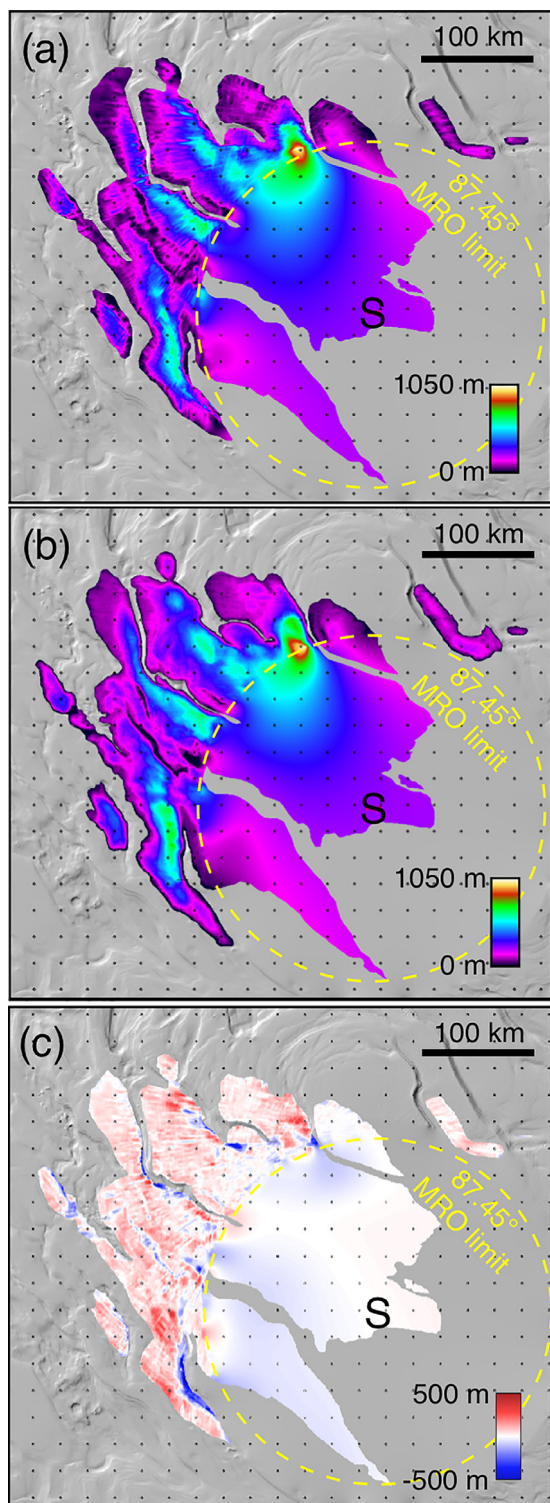


Fig. 5. Maps of CO_2 ice thickness in Australe Mensa using (a) a collection of 429 SHARAD 2-D profiles (Bierson et al., 2016) and (b) using the SHARAD 3-D volume, and (c) the difference between the 3-D and 2-D thickness maps. Orbit-track-aligned lineations and patchwork in the 2-D thickness map are largely the result of interpolation. The improved 3-D imaging of subsurface structures provides more confidence in locating the deposit and in estimating the volume of CO_2 ice, which we find to be $16,500 \text{ km}^3$ (11% larger than the 2-D-based result).

partially buried craters. We find similar signatures elsewhere in both volumes but without surface expression (e.g., circled features in Figs. 2 and 3). Presumably fully buried craters, these features provide a potential means to constrain the ages of both the

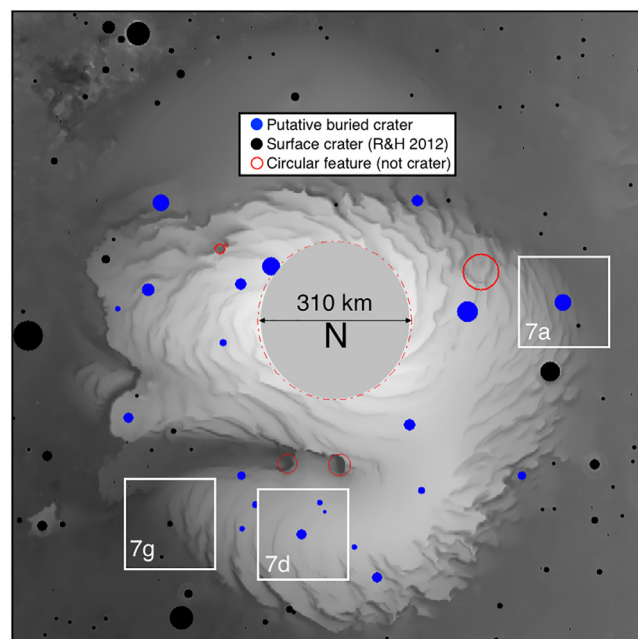


Fig. 6. Locations of craters larger than 4 km in diameter as previously mapped with surface data (black circles; Robbins and Hynek, 2012) and of apparent buried craters (blue circles) that we mapped in the Planum Boreum 3-D radar volume at the base of the NPLD. We found six Robbins and Hynek (2012) features (red circles) to be questionable as craters and omitted them from our analysis (Fig. 8). Circles are scaled to the maximum diameters of each feature. White boxes show bounds of radar views in Fig. 7 of the apparent or known crater at the center of each box. Base map is MOLA 128-ppd elevation (Smith et al., 2003) (black low, white high). (For interpretation of the references to color in this figure legend, the reader is referred to the web version of this article.)

substrate and the overlying icy deposits that is independent of climate models. Identification of such apparent buried craters throughout the radar volumes is ongoing. Because the 3-D imaging process involves the use of a hyperbolic operator, hyperboloid (bowl-shaped) processing artifacts appear in the volumes, typically where radar coverage of features is incomplete. Given that craters are themselves bowl-shaped structures, one must take care to avoid mistaking such artifacts for buried craters. Since the material properties in the subsurface are assumed to be constant for the imaging process, the expected shape of isolated processing artifacts is well known, and this fact can be used to help discriminate artifacts from true structures.

For this work, we report our initial efforts to identify apparent craters at the base of the NPLD in Planum Boreum. We have identified and mapped 21 of these features (see map in Fig. 6, radar examples in Fig. 7, and data in Table 1), ranging in size from 7 to 45 km in diameter. Smaller craters are difficult to resolve with the 475-m grid size of the 3-D volume. The materials underlying the NPLD are believed to be either the same as those in the surrounding plains or consisting of sand-rich basal deposits, which have been interpreted to have a similar age (i.e., the Hesperian “Vastitas Borealis interior” geologic unit in the surroundings and the Hesperian “rupeS,” and “cavi” geologic units at the base; Tanaka and Fortezzo, 2012). Therefore, we compared our set of apparent craters to surface craters mapped previously in the polar region (Robbins and Hynek, 2012). In Fig. 8, we present cumulative size-frequency distributions for our set alone, for our set combined with surface craters in the same area (80°N – 87.5°N), and for surface craters in the surrounding region (70°N – 80°N) along with isochrons for various ages (Hartmann, 2005). In our analysis, we omit six features on Planum Boreum marked as surface craters by Robbins and Hynek (2012), having found no clear evidence of

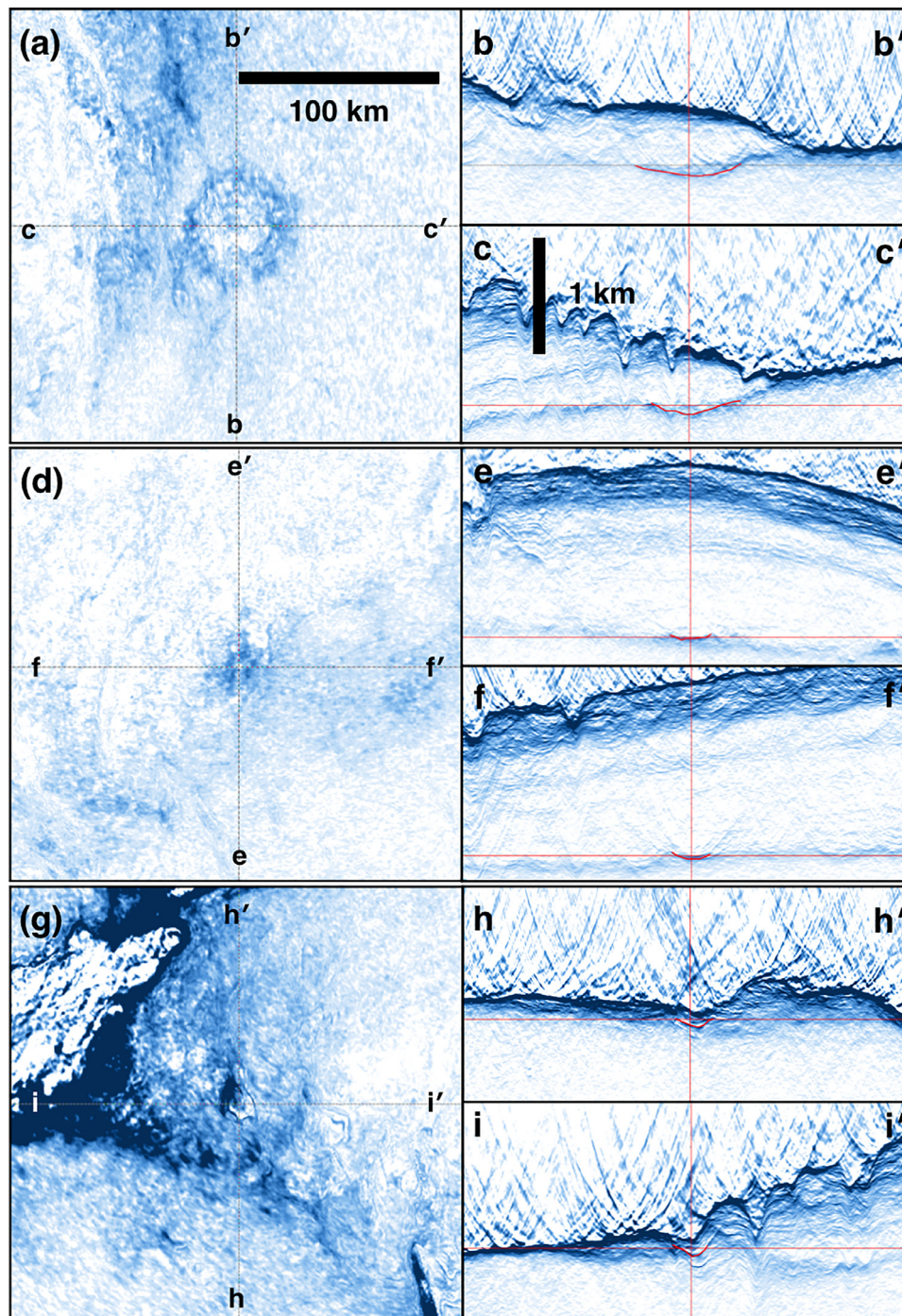


Fig. 7. SHARAD 3-D radar views of (a–f) two apparent fully buried craters and (g–i) one partially buried, known crater, showing (a, d, g) constant-depth slices, (b, e, h) inline profiles aligned with 0–180 °E, and (c, f, i) crossline profiles aligned with 270–90 °E. Bold red lines on each profile show interpreted extents of crater. Traces of orthogonal views align with cross-hairs in each panel and scale bars apply to all panels. See Fig. 6 for location of depth slices. (For interpretation of the references to color in this figure legend, the reader is referred to the web version of this article.)

crater morphology in current high-resolution imagery. In general, we find a good agreement between the sets of craters, suggesting that the features we mapped are indeed buried craters present in units of the same age as that of the surrounding plains. At the smallest size bins, the distribution of apparent buried crater rolls off quickly, an indication of the lower limit of resolution where we were able to identify them in the radar volume. This first result lends some confidence to our ongoing effort to identify and map other buried craters within the overlying NPLD and in the south polar 3-D volume. Given the relatively young age of the NPLD

suggested by climate modeling results (e.g., [Levrard et al., 2007](#)) and our limits of feature-size detectability, there may be too few apparent craters available within the icy layered deposits for a reliable age determination. A preliminary look at the Planum Australe volume suggests that there are many more apparent buried craters within the SPLD than within the NPLD, likely reflecting a greater age and perhaps a sufficient number to provide a reliable cratering age.

As noted above, the 3-D imaging process correctly positions radar returns from features that are well sampled, and this

Table 1
Sizes and locations of apparent fully buried craters at base of NPLD.

Max. diam. (km)	Min. diam. (km)	Latitude (°N)	Longitude (°E)	Elevation ^a (m)	Depth (m)
45.3	39.0	85.142	94.159	-4621	1671
41.0	35.2	86.872	-130.547	-1011	1571
38.0	24.9	82.241	-124.299	-4237	193
37.5	36.6	81.627	94.746	-3591	589
29.2	28.4	83.024	-99.549	-2932	617
26.0	22.4	84.628	146.064	-4165	145
25.0	23.8	86.246	-111.275	-1657	1159
23.9	22.0	85.303	35.438	-1297	1624
22.8	21.8	82.025	-8.989	-1816	1564
22.7	20.7	80.432	9.181	-2066	1388
21.9	20.9	81.596	-64.877	-3747	144
17.6	17.3	83.316	-31.256	-3550	758
17.3	16.5	81.103	50.096	-3813	431
17.0	11.1	85.800	-78.893	-1816	1070
16.1	15.5	82.603	-23.431	-2376	1350
14.7	14.5	82.990	26.772	-1292	1764
14.1	13.8	81.598	-24.158	-2442	1328
11.8	11.7	83.282	-4.919	-1874	1536
11.5	11.2	81.628	4.810	-1467	1717
11.4	9.4	82.007	-93.365	-3845	186
7.3	6.6	82.939	-3.201	-1684	1624

^a Elevations measured at deepest point near the center of each apparent crater.

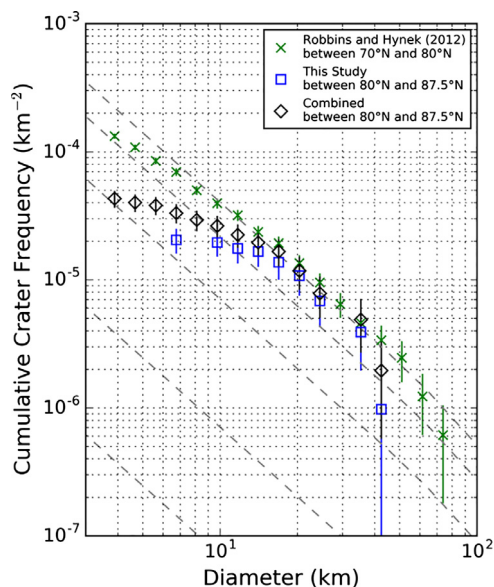


Fig. 8. The cumulative size-frequency distribution of the apparent fully buried craters at the base of the NPLD (blue squares) matches well with that of previously mapped surface craters (Robbins and Hynek, 2012) in terrains surrounding Planum Boreum (green crosses) for diameters between 15 and 35 km. When the apparent buried craters and known surface craters within Planum Boreum are taken together (black diamonds), the correspondence improves. Isochrons (dashed lines, Hartmann, 2005) from lower left to upper right are for 10, 100, 1000, 3000, and 3500 Ma. Vertical lines show 1- σ confidence intervals. See Fig. 6 for crater locations. (For interpretation of the references to color in this figure legend, the reader is referred to the web version of this article.)

applies to surface reflections as well as to subsurface ones. SHARAD coverage is very dense at the highest latitudes reached in MRO's orbit, and this allows us to produce maps of surface topography in addition to mapping subsurface features. While the lateral resolution of SHARAD is inferior to that of the Mars Orbiter Laser Altimeter (MOLA) onboard Mars Global Surveyor (MGS), MRO reached higher latitudes than MGS. Thus we are able to derive topographic maps for both polar regions between the maximum latitudes reached by MGS and MRO. In areas with equator-facing slopes, these maps extend somewhat poleward of the MRO maximum latitude due to off-nadir sampling by SHARAD that is cor-

rected into these areas by the 3-D imaging process. In areas with pole-facing slopes, there are gaps where no returns are obtained by SHARAD. In Fig. 9, we present revised topographic maps of the polar regions as extensions of the MOLA 128-pixel-per-degree gridded maps (Smith et al., 2003) using the SHARAD-derived topography. In addition to providing new topographic data in a total area of 28,500 km² for both poles, the improvement in topography will also be of benefit for creating more accurate clutter simulations (e.g., Choudhary et al., 2016) along the tracks of individual SHARAD polar observations.

In the course of assembling SHARAD observations into a 3-D volume, it was discovered that the delay to the surface at track intersections differs between observations taken on different orbits (Foss et al., 2017). The problem was found to pervade the entire SHARAD dataset (polar and non-polar) and has multiple causes, one of which is variable spacecraft-to-surface delay times at the same locale due to the constantly changing state of the ionosphere (Campbell et al., 2011). While a means was developed to account for the majority of the delay offsets (Campbell et al., 2014), residual delays remain in both volumes. These residuals combined with incomplete coverage in the 475-m \times 475-m binning grids impact the quality of the 3-D volumes, most notably by reducing the effective vertical resolution by a factor of ~ 2 relative to the input 2-D radargrams. Specifically, finer shallow layering and smaller structures evident in the input 2-D observations are not resolved as well in the 3-D volume (see Fig. 4). This loss of resolution hampers the ability to improve upon prior efforts to correlate radar layering with that seen in visible imagery (e.g., Milkovich et al., 2009; Phillips et al., 2009; Christian et al., 2013), to map minor troughs and near-surface undulations linked to climate signals (e.g., Smith and Holt, 2015; Smith et al., 2016), and to visualize small structures. As noted above, another limitation of the radar volume is the incomplete correction of clutter in areas with SHARAD coverage that is coarser than the 3-D grid size. A continuing effort will attempt to reduce the residual delays, and SHARAD data acquisition is ongoing with a goal of infilling coverage in areas targeted for 3-D processing. Additional processing improvements are being considered and may enable mapping of changes in dielectric properties within the volumes, among other improvements (Foss et al., 2017). In the meantime, these first 3-D volumes provide superior imaging of the larger-scale features and views of the data that are not possible with the collection of 2-D profiles (e.g., slices and transects through the volumes in any direction). These factors

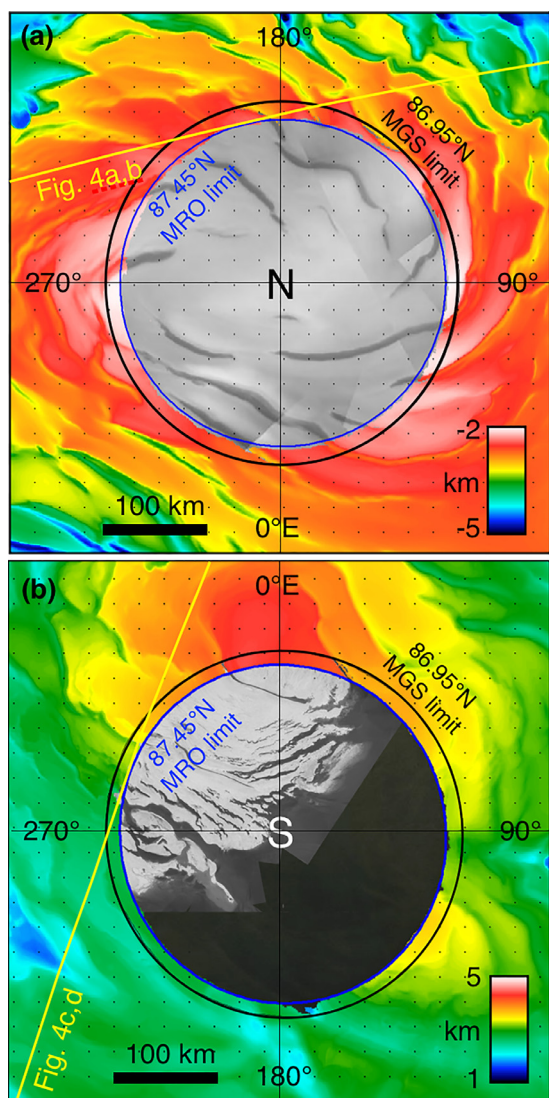


Fig. 9. Topography of (a) Planum Boreum and (b) Planum Australe. At latitudes below the highest reached by MGS (black circles, $\sim 86.95^\circ$), the maps show MOLA 128-pixel-per-degree gridded topography (Smith et al., 2003). At higher latitudes up to the highest reached by MRO (blue circles, $\sim 87.45^\circ$) the maps show SHARAD-derived topography in a total area of 28,500 km². The SHARAD data show fidelity to finer structures (e.g., undulations at 87°N , 265°E) and data drop-outs or poleward excursions in steeply dipping terrains. Image mosaics inside the MRO circles are from (a) Viking MDIM and (b) MRO CTX (courtesy of Peter Thomas). (For interpretation of the references to color in this figure legend, the reader is referred to the web version of this article.)

allow refinement of previously mapped feature boundaries and the discovery of new features, such as the apparent buried craters.

5. Conclusions

SHARAD observations on thousands of orbital passes by MRO over Planum Boreum and Planum Australe have enabled the construction of 3-D data volumes encompassing the Martian polar ice caps. Each volume has undergone 3-D migration processing, an imaging method that corrects off-nadir returns (clutter) and properly positions internal structures while improving the overall SNR (Foss et al., 2017). Clutter mitigation and the structural corrections that migration provides have been particularly effective, supporting the mapping of a shallow unconformity linked to the most recent retreat of mid-latitude glaciation (Smith et al., 2016) and an improved volume estimate for buried CO₂ ice discovered with 2-D

profiles. In addition, the clarified view provided by the 3-D volumes reveals what appear to be impact craters fully buried below and within the icy layered deposits. In a first effort to map them in the radar data, we find 21 of these features at the base of the NPLD with diameters between 7 km and 45 km, consistent with the size and distribution of surface craters in the surrounding plains. A more complete assessment of buried craters within both PLDs may provide new constraints on the ages of these deposits that is independent of climate models, but detecting a statistically sufficient number for accurate cratering dates may be challenging due to the expected relatively young age of the deposits. In general, the clarified views of the polar-cap interiors emerging from the polar SHARAD 3-D volumes is enhancing our ability to map interior structures and infer the history of their emplacement. Ongoing work to improve the vertical resolution and coverage for polar SHARAD volumes is likely to yield more insights and discoveries, allowing more advancement toward the overarching goal of linking the geologic history of the polar deposits to climate processes and their history.

Acknowledgments

The SHARAD instrument was provided to NASA's MRO mission by the Italian Space Agency (ASI), and its operations are led by the DIET Department, University of Rome "La Sapienza" under an ASI contract. We are grateful to the MRO Project and the SHARAD Team for supporting the 3-D projects and to SeisWare, Inc. for access to the interpretation software used for the analysis and displays of radar data and mapping results presented here. Reviews by Joseph MacGregor and an anonymous reviewer greatly improved the manuscript. This work was funded by the Mars Data Analysis Program through NASA Grants NNX10AQ32G, NNX13AK77G, and NNX17AC62G. Binary forms of the 3-D data volumes will be made available on the Geosciences node of the Planetary Data System (PDS) from the SHARAD archive page at <http://pds-geosciences.wustl.edu/missions/mro/sharad.htm>. Animations and SEG-Y formatted data currently available at <http://sharad.psi.edu/3D> will be included as PDS supplemental products.

References

- Bednar, J.B., 2005. A brief history of seismic migration. *Geophysics* 70, 3MJ–20MJ. doi:10.1190/1.1926579.
- Bierson, C.J., Phillips, R.J., Smith, I.B., Wood, S.E., Putzig, N.E., Nunes, D., Byrne, S., 2016. Stratigraphy and evolution of the buried CO₂ deposit in the Martian south polar cap. *Geophys. Res. Lett.* 43, 4172–4179.
- Brothers, T.C., Holt, J.W., Spiga, A., 2015. Planum Boreum basal unit topography, Mars: irregularities and insights from SHARAD. *J. Geophys. Res.* 120, 1357–1375. doi:10.1002/2015JE004830.
- Byrne, S., 2009. The polar deposits of Mars. *Annu. Rev. Earth Planet. Sci.* 37, 535–560. doi:10.1146/annurev.earth.031208.100101.
- Byrne, S., Murray, B.C., 2002. North polar stratigraphy and the paleo-erg of Mars. *J. Geophys. Res.* 107, 5044. doi:10.1029/2001JE001615.
- Campbell, B., Carter, L., Phillips, R., Plaut, J., Putzig, N., Safaeinili, A., Seu, R., Biccardi, D., Egan, A., Orosei, R., 2008. SHARAD radar sounding of the Vastitas Borealis Formation in Amazonis Planitia. *J. Geophys. Res.* 113, E12010. doi:10.1029/2008JE003177.
- Campbell, B.A., Morgan, G.A., Putzig, N.E., Whitten, J.L., Holt, J.W., Phillips, R.J., 2015. Enhanced radar visualization of structure in the south polar deposits of Mars. In: *Proceedings of XLVth Lunar Planetary Science Abstract* 2366.
- Campbell, B.A., Phillips, R.J., 2014. Mars Reconnaissance Orbiter Shallow Radar Radargram Data. NASA Planetary Data System, MRO-M-SHARAD-5-RADARGRAM-V1.0. NASA http://pds-geosciences.wustl.edu/mro/mro-m-sharad-5-radargram-v1/mrosh_2001/.
- Campbell, B.A., Putzig, N.E., Carter, L.M., Phillips, R.J., 2011. Autofocus correction of phase distortion effects on SHARAD echoes. *IEEE Geosci. Remote Sens. Lett.* 8, 939–942. doi:10.1109/LGRS.2011.2143692.
- Campbell, B.A., Putzig, N.E., Foss II, F.J., Phillips, R.J., 2014. SHARAD signal attenuation and delay offsets due to the martian ionosphere. *IEEE Geosci. Remote Sens. Lett.* 11, 632–635. doi:10.1109/LGRS.2013.2273396.
- Choudhary, P., Holt, J.W., Kempf, S.D., 2016. Surface clutter and echo location analysis for the interpretation of SHARAD data from Mars. *IEEE Geosci. Remote Sens. Lett.* 13, 1285–1289. doi:10.1109/LGRS.2016.2581799.

- Christian, S., Holt, J.W., Byrne, S., Fishbaugh, K.E., 2013. Integrating radar stratigraphy with high resolution visible stratigraphy of the north polar layered deposits, Mars. *Icarus* 226, 1241–1251. doi:10.1016/j.icarus.2013.07.003.
- Claerbout, J.F., 1985. *Imaging the Earth's Interior*. Blackwell Scientific Publications, Oxford, UK, p. 398.
- Fishbaugh, K.E., Head, J.W., 2005. Origin and characteristics of the Mars north polar basal unit and implications for polar geologic history. *Icarus* 174, 444–474. doi:10.1016/j.icarus.2004.06.021.
- Foss II, F.J., Putzig, N.E., Campbell, B.A., Phillips, R.J., 2017. 3-D imaging of Mars' polar ice caps using orbital radar data. *The Leading Edge* 36, 43–57. doi:10.1190/tle36010043.1.
- French, W.S., 1974. Two-dimensional and three-dimensional migration of model-experiment reflection profiles. *Geophysics* 39, 265–277. doi:10.1190/1.1440426.
- Gazdag, J., 1978. Wave equation migration with the phase-shift method. *Geophysics* 43, 1342–1351.
- Gray, S.H., Etgen, J., Dellinger, J., Whitmore, D., 2001. Seismic migration problems and solutions. *Geophysics* 66, 1622–1640.
- Grima, C., Kofman, W., Mouginot, J., Phillips, R.J., Hérique, A., Biccari, D., Seu, R., Cutigni, M., 2009. North polar deposits of Mars: extreme purity of the water ice. *Geophys. Res. Lett.* 36, 4. doi:10.1029/2008GL036236, L03203.
- Hartmann, W.K., 2005. Martian cratering 8: Isochron refinement and the chronology of Mars. *Icarus* 174, 294–320. doi:10.1016/j.icarus.2004.11.023.
- Holt, J.W., Fishbaugh, K.E., Byrne, S., Christian, S., Tanaka, K., Russell, P.S., Herkenhoff, K.E., Safaeinili, A., Putzig, N.E., Phillips, R.J., 2010. The construction of Chasma Boreale on Mars. *Nature* 465, 446–449. doi:10.1038/nature09050.
- Holt, J.W., Safaeinili, A., Plaut, J.J., Head, J.W., Phillips, R.J., Seu, R., Kempf, S.D., Choudhary, P., Young, D.A., Putzig, N.E., 2008. Radar sounding evidence for buried glaciers in the southern mid-latitudes of Mars. *Science* 322, 1235–1238. doi:10.1126/science.1164246.
- Laskar, J., Levrard, B., Mustard, J.F., 2002. Orbital forcing of the Martian polar layered deposits. *Nature* 419, 375–377.
- Levrard, B., Forget, F., Montmessin, F., Laskar, J., 2007. Recent formation and evolution of northern Martian polar layered deposits as inferred from a Global Climate Model. *J. Geophys. Res.* 112, 18. doi:10.1029/2006JE002772, E06012.
- Liner, C., 2016. *Elements of 3D Seismology*. Society of Exploration Geophysics, Tulsa, OK, p. 362.
- Maxwell, T.A., Phillips, R.J., 1978. Stratigraphic correlation of the radar-detected subsurface interface in Mare Crisium. *Geophys. Res. Lett.* 5, 811–814.
- Milkovich, S.M., Plaut, J.J., Safaeinili, A., Picardi, G., Seu, R., Phillips, R.J., 2009. Stratigraphy of Prometheus Lingula, south polar layered deposits, Mars, in radar and imaging data sets. *J. Geophys. Res.* 114, E03002. doi:10.1029/2008JE003162.
- Nerozzi, S., Holt, J.W., 2017. Earliest accumulation history of the north polar layered deposits, Mars from SHARAD. *Icarus* doi:10.1016/j.icarus.2017.05.027, in press.
- Nunes, D.C., Phillips, R.J., 2006. Radar subsurface mapping of the polar layered deposits on Mars. *J. Geophys. Res.* 111, E06S21. doi:10.1029/2005JE002609.
- Peeples, W.J., Sill, W.R., May, T.W., Ward, S.H., Phillips, R.J., Jordan, R.L., Abbott, E.A., Killpack, T.J., 1978. Orbital radar evidence for lunar subsurface layering in Maria Serenitatis and Crisium. *J. Geophys. Res.* 83, 3459–3468.
- Phillips, R.J., Davis, B.J., Tanaka, K.L., Byrne, S., Mellon, M.T., Putzig, N.E., Haberle, R.M., Kahre, M.A., Campbell, B.A., Carter, L.M., 2011. Massive CO₂ ice deposits sequestered in the south polar layered deposits of Mars. *Science* 332, 838–841. doi:10.1126/science.1203091.
- Phillips, R.J., Putzig, N.E., Head, J.W., Egan, A.F., Plaut, J.J., Safaeinili, A., Smrekar, S.E., Milkovich, S.M., Nunes, D.C., Campbell, B.A., Carter, L.M., Holt, J.W., Seu, R., Orosei, R., 2009. Subsurface structure of the south polar layered deposits, Mars. In: *Proceedings of XLth Lunar Planetary Science Abstract 2007*.
- Phillips, R.J., Zuber, M.T., Smrekar, S.E., Mellon, M.T., Head, J.W., Tanaka, K.L., Putzig, N.E., Milkovich, S.M., Campbell, B.A., Plaut, J.J., Safaeinili, A., Seu, R., Biccari, D., Carter, L.M., Picardi, G., Orosei, R., Mohit, P.S., Heggy, E., Zurek, R.W., Egan, A.F., Giacomoni, E., Russo, F., Cutigni, M., Pettinelli, E., Holt, J.W., Leuschen, C.J., Marinangeli, L., 2008. Mars north polar deposits: stratigraphy, age, and geodynamical response. *Science* 320, 1182–1185. doi:10.1126/science.1157546.
- Picardi, G., Plaut, J.J., Biccari, D., Bombaci, O., Calabrese, D., Cartacci, M., Cicchetti, A., Clifford, S.M., Edenhofer, P., Farrell, W.M., Federico, C., Frigeri, A., Gurnett, D.A., Hagfors, T., Heggy, E., Hérique, A., Huff, R.L., Ivanov, A.B., Johnson, W.T.K., Jordan, R.L., Kirchner, D.L., Kofman, W., Leuschen, C.J., Nielsen, E., Orosei, R., Pettinelli, E., Phillips, R.J., Plettemeier, D., Safaeinili, A., Seu, R., Stofan, E.R., Vannaroni, G., Watters, T.R., Zampolini, E., 2005. Radar soundings of the subsurface of Mars. *Science* 310, 1925–1928.
- Plaut, J.J., Picardi, G., Safaeinili, A., Ivanov, A.B., Milkovich, S.M., Cicchetti, A., Kofman, W., Mouginot, J., Farrell, W.M., Phillips, R.J., Clifford, S.M., Frigeri, A., Orosei, R., Federico, C., Williams, I.P., Gurnett, D.A., Nielsen, E., Hagfors, T., Heggy, E., Stofan, E.R., Plettemeier, D., Watters, T.R., Leuschen, C.J., Edenhofer, P., 2007. Subsurface radar sounding of the south polar layered deposits of Mars. *Science* 316, 92–95.
- Putzig, N.E., Phillips, R.J., Campbell, B.A., Holt, J.W., Plaut, J.J., Carter, L.M., Egan, A.F., Bernardini, F., Safaeinili, A., Seu, R., 2009. Subsurface structure of Planum Boreum from Mars reconnaissance orbiter shallow radar soundings. *Icarus* 204, 443–457. doi:10.1016/j.icarus.2009.07.034.
- Robbins, S.J., Hynes, B.M., 2012. A new global database of Mars impact craters ≥ 1 km: 2. Global crater properties and regional variations of the simple-to-complex transition diameter. *J. Geophys. Res.* 117, E06001. doi:10.1029/2011JE003967, 10.1029/2011JE003967.
- Selvans, M.M., Plaut, J.J., Aharonson, O., Safaeinili, A., 2010. Internal structure of Planum Boreum, from Mars advanced radar for subsurface and ionospheric sounding data. *J. Geophys. Res.* 115, 9 pages. doi:10.1029/2009JE003537.
- Seu, R., Phillips, R.J., Alberti, G., Biccari, D., Bonaventura, F., Bortone, M., Calabrese, D., Campbell, B.A., Cartacci, M., Carter, L.M., Catalo, C., Croce, A., Croci, R., Cutigni, M., Di Placido, A., Dinardo, S., Federico, C., Flamini, E., Fois, F., Frigeri, A., Fuga, O., Giacomoni, E., Gim, Y., Guelfi, M., Holt, J.W., Kofman, W., Leuschen, C.J., Marinangeli, L., Marras, P., Masdea, A., Mattei, S., Mecozzi, R., Milkovich, S.M., Morlupi, A., Mouginot, J., Orosei, R., Papa, C., Paterno, T., Persi del Marmo, P., Pettinelli, E., Pica, G., Picardi, G., Plaut, J.J., Provenziani, M., Putzig, N.E., Russo, F., Safaeinili, A., Salzillo, G., Santovito, M.R., Smrekar, S.E., Tattarletti, B., Vicari, B., 2007a. Accumulation and erosion of Mars' south polar layered deposits. *Science* 317, 1715–1718. doi:10.1126/science.1144120.
- Seu, R., Phillips, R.J., Biccari, D., Orosei, R., Masdea, A., Picardi, G., Safaeinili, A., Campbell, B.A., Plaut, J.J., Marinangeli, L., Smrekar, S.E., Nunes, D.C., 2007b. SHARAD sounding radar on the Mars Reconnaissance Orbiter. *J. Geophys. Res.* 112, E05S05. doi:10.1029/2006JE002745.
- Smith, D., Neumann, G., Arvidson, R.E., Guinness, E.A., Slavney, S., 2003. Mars Global Surveyor Laser Altimeter Mission Experiment Gridded Data Record. NASA Planetary Data System MGS-MOLA-5-MEGDR-L3-V1.0. NASA.
- Smith, I.B., Holt, J.W., 2010. Onset and migration of spiral troughs on Mars revealed by orbital radar. *Nature* 465, 450–453.
- Smith, I.B., Holt, J.W., 2015. Spiral trough diversity on the north pole of Mars, as seen by Shallow Radar (SHARAD). *J. Geophys. Res.* 120, 362–387. doi:10.1002/2014JE004720.
- Smith, I.B., Holt, J.W., Spiga, A., Howard, A.D., Parker, G., 2013. The spiral troughs of Mars as cyclic steps. *J. Geophys. Res.* 118, 1835–1857. doi:10.1002/jgre.20142.
- Smith, I.B., Putzig, N.E., Holt, J.W., Phillips, R.J., 2016. An ice age recorded in the polar deposits of Mars. *Science* 352, 1075–1078. doi:10.1126/science.aad6968.
- Stolt, R.H., 1978. Migration by Fourier transform. *Geophysics* 43, 23–48.
- Tanaka, K.L., Fortezzo, C.M., 2012. *Geologic Map of the North Polar Region of Mars*. USGS Scientific Investigations Map 3177. USGS.
- Watters, T.R., Campbell, B., Carter, L., Leuschen, C.J., Plaut, J.J., Picardi, G., Orosei, R., Safaeinili, A., Clifford, S.M., Farrell, W.M., 2007. Radar sounding of the Medusae Fossae formation Mars: equatorial ice or dry, low-density deposits? *Science* 318, 1125.
- Yilmaz, O., 1987. *Seismic Data Processing*. Society of Exploration Geophysics, Tulsa, OK, p. 526.
- Yilmaz, O., Chambers, R., Nichols, D., Abma, R., 1987a. Fundamentals of 3-D migration: part 1. *Geophys.: The Leading Edge Explor.* 6, 22–30.
- Yilmaz, O., Chambers, R., Nichols, D., Abma, R., 1987b. Fundamentals of 3-D migration: part 2. *Geophys.: The Leading Edge Explor.* 6, 26–33.